

# Accepted Manuscript

Multi-locus transcranial magnetic stimulation—theory and implementation

Lari M. Koponen, Jaakko O. Nieminen, Risto J. Ilmoniemi

PII: S1935-861X(18)30097-4

DOI: [10.1016/j.brs.2018.03.014](https://doi.org/10.1016/j.brs.2018.03.014)

Reference: BRS 1222

To appear in: *Brain Stimulation*

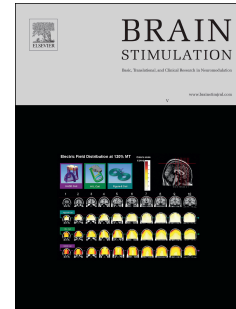
Received Date: 3 November 2017

Revised Date: 9 February 2018

Accepted Date: 20 March 2018

Please cite this article as: Koponen LM, Nieminen JO, Ilmoniemi RJ, Multi-locus transcranial magnetic stimulation—theory and implementation, *Brain Stimulation* (2018), doi: 10.1016/j.brs.2018.03.014.

This is a PDF file of an unedited manuscript that has been accepted for publication. As a service to our customers we are providing this early version of the manuscript. The manuscript will undergo copyediting, typesetting, and review of the resulting proof before it is published in its final form. Please note that during the production process errors may be discovered which could affect the content, and all legal disclaimers that apply to the journal pertain.



# Multi-locus transcranial magnetic stimulation—theory and implementation

Lari M. Koponen<sup>a,b,1</sup>, Jaakko O. Nieminen<sup>a,b,1,\*</sup>, and Risto J. Ilmoniemi<sup>a,b</sup>

<sup>a</sup>Department of Neuroscience and Biomedical Engineering, Aalto University School of Science, P.O. Box 12200, FI-00076 AALTO, Espoo, Finland

<sup>b</sup>BioMag Laboratory, HUS Medical Imaging Center, University of Helsinki and Helsinki University Hospital, P.O. Box 340, FI-00029 HUS, Helsinki, Finland

<sup>1</sup>These authors contributed equally to this work.

\*Corresponding author: Jaakko O. Nieminen, jaakko.nieminen@aalto.fi, Department of Neuroscience and Biomedical Engineering, Aalto University School of Science, P.O. Box 12200, FI-00076 AALTO, Espoo, Finland

## 12 Abstract

13 *Background:* Transcranial magnetic stimulation (TMS) is a non-invasive brain stimulation method: a  
14 magnetic field pulse from a TMS coil can excite neurons in a desired location of the cortex. Conventional  
15 TMS coils cause focal stimulation underneath the coil centre; to change the location of the stimulated spot,  
16 the coil must be moved over the new target. This physical movement is inherently slow, which limits, for  
17 example, feedback-controlled stimulation.

18 *Objective:* To overcome the limitations of physical TMS coil movement by introducing electronic targeting.

19 *Methods:* We propose electronic stimulation targeting using a set of large overlapping coils and introduce a  
20 matrix-factorisation-based method to design such sets of coils. We built one such device and demonstrated  
21 the electronic stimulation targeting *in vivo*.

22 *Results:* The demonstrated two-coil transducer allows translating the stimulated spot along a 30-mm line  
23 segment in the cortex; with five coils, a target can be selected from within a region of the cortex and  
24 stimulated in any direction. Thus, far fewer coils are required by our approach than by previously suggested  
25 ones, none of which have resulted in practical devices.

26 *Conclusion:* Already with two coils, we can adjust the location of the induced electric field maximum along  
27 one dimension, which is sufficient to study, for example, the primary motor cortex.

## 28 Keywords

29 Transcranial magnetic stimulation, multi-channel TMS, multi-locus TMS, instrumentation, coil design,  
30 electric field

31

## 32 Introduction

33 Transcranial magnetic stimulation (TMS) is a method for non-invasive brain stimulation [1]. It has become  
34 an attractive tool in neuroscience [2, 3, 4] and in some clinical applications [5, 6], with thousands of devices  
35 worldwide. In TMS, a strong current pulse through the windings of a coil produces a magnetic field, which,  
36 in turn, induces an electric field (E-field) in nearby tissues. With a suitable figure-of-eight coil [7], the cortex  
37 can be stimulated locally; a typical modern TMS device has one such coil, held at the desired position above  
38 the stimulation target. Neuronavigation technology [8, 9, 10], with targeting based on individual anatomical  
39 images and with visual feedback to the operator, makes it relatively straightforward to maintain the  
40 stimulated spot (i.e., the location of the E-field maximum in the cortex) within one or two millimetres of its  
41 desired location (the stimulation target). Even neuronavigated conventional TMS devices have, however, a  
42 major limitation: to change the stimulated spot, the coil must be moved. Moving the heavy (around 1–2 kg)  
43 coil, even robotically [11], is relatively slow, as the coil must be close to the scalp during the stimulation and  
44 safety has to be guaranteed. Thus, when connectivity between cortical areas has been studied with TMS  
45 pulses targeted to them in a sequence, two [12] or sometimes even three [13] distinct coils have been  
46 used—one for each stimulation target.

47 Although multiple spots can be stimulated in quick succession with multiple separate coils, this approach  
48 has severe limitations. First, it is cumbersome to manipulate and control several coils at the same time.  
49 Second, the large size of the coils makes it difficult to stimulate nearby cortical locations [14, 15]. Third,  
50 changing any of the stimulated spots still requires a rearrangement of the coil assembly. To overcome these  
51 limitations, the concept of an array of small coils has been suggested [8, 16]. With such an array, the  
52 stimulated spot could, in principle, be changed electronically without moving the coils. The previously  
53 proposed approach, however, would require a large number of coils (a rectangular 4-by-4 lattice of 16 coils,  
54 each smaller than 30 mm in diameter, could cover a region slightly smaller than the four central coils) and  
55 much more power to drive all the coils than is required for a single conventional TMS coil. Indeed, each  
56 such coil would require its own power electronics similar to that of a conventional TMS device. As a TMS

57 device is largely characterised by its power electronics, this essentially means that at least 16 TMS devices  
 58 would be required to drive such an array. This would make the device both costly and bulky; to our  
 59 knowledge, no such device has ever been built. The largest multi-channel TMS device described in the  
 60 literature has five coils and is intended to give multiple simultaneous pulses with different waveforms [17].  
 61 In this work, we propose and demonstrate a practical approach to control the stimulated spot within the  
 62 cortex and provide an algorithm to design multi-locus TMS (mTMS) transducers with overlapping coils. As  
 63 will be shown in this study, with five such coils, one can select a target location from within a region of the  
 64 cortex and stimulate it in any desired direction, and, with just two coils, one obtains adequate control over  
 65 the target location to scan the primary motor cortex (M1) without coil movement. To demonstrate  
 66 practical electronic targeting, we built such a two-coil mTMS device and applied it to M1 *in vivo*.

## 67 Material and methods

### 68 Transducer design algorithm

69 For the design of mTMS transducers, we propose an algorithm that gives a close-to-minimum number of  
 70 coils to obtain the desired degrees of freedom for electronic control of the characteristics of the E-field,  
 71 such as the location of its maximum. The algorithm translates the problem into a matrix form and uses  
 72 known matrix factorisation methods to minimise the number of coils needed to meet given specifications.

73 An  $N$ -channel mTMS transducer consists of a set of  $N$  coil windings, each with a different pattern of  
 74 induced E-field. To find a suitable set of  $N$  coils, we first specify the spatial stimulation patterns the  
 75 transducer should be able to produce. For simplicity, we define each stimulation pattern by the maximum  
 76 induced E-field,  $\mathbf{E}_{\text{target}}$  obtained at location  $\mathbf{x}_{\text{target}}$ , and its focality, that is, the extent of  $N_{\text{ROI}}$  regions  
 77 outside of which the E-field magnitude is below certain thresholds [18]:

$$\mathbf{E}(\mathbf{x}_{\text{target}}) = \mathbf{E}_{\text{target}},$$

$$\forall \mathbf{x} : |\mathbf{E}(\mathbf{x})| \leq |\mathbf{E}_{\text{target}}|,$$

78 and

$$\forall \mathbf{x} \notin \text{ROI}_i : |\mathbf{E}(\mathbf{x})| \leq c_i |\mathbf{E}_{\text{target}}| .$$

79 ROI<sub>*i*</sub> specifies the *i*:th region (*i* = 1 ... *N*<sub>ROI</sub>) and 0 < *c*<sub>*i*</sub> < 1 describes how much the E-field amplitude is  
 80 reduced outside it. For example, to design a transducer that is able to induce an equally focal E-field  
 81 distribution in any orientation in any location within a continuous region of interest, we could form a nearly  
 82 uniform grid of target locations and a set of equally spaced stimulation orientations for each target. When  
 83 the discretised set of stimulation patterns has a sufficient sampling density, this set allows approximating a  
 84 continuous set of target locations and orientations.

85 If we assume that the *N* coils forming the mTMS transducer are contained within one thin layer, each of  
 86 them can be described in a common basis: as with our previous work, a coil is described by its stream  
 87 function lying on a surface that follows the overall transducer shape and covers the whole transducer [19].  
 88 At this point, we define the overall shape of the transducer, e.g., planar or curved, and its dimensions. A  
 89 stream function describes the amount of current around each point; any coil-current pattern can be  
 90 approximately represented by an *n*-dimensional vector, *c*, where *n* is the number of interior vertices in the  
 91 triangular mesh used to discretise the surface. Next, we look for a set of coil-current patterns on the  
 92 transducer surface that can induce all required stimulation patterns. The final *N* stream functions that  
 93 correspond to the *N* coils of the transducer must span this set of coil-current patterns. We can obtain one  
 94 possible set by computing the minimum-energy TMS coils, that is, solving the convex single-coil  
 95 optimisation problem of Ref. [19], for all *m* specified stimulation patterns separately:

$$\arg \min_{\mathbf{c}_i \in C_i} \iiint |\mathbf{B}_{\mathbf{c}_i}(\mathbf{x})|^2 d\mathbf{x}^3 ,$$

96 where *c*<sub>*i*</sub> is the minimum-energy coil from the set of all coils that satisfy the *i*:th pattern (*C*<sub>*i*</sub>), *x* is a point in  
 97 space, *B*<sub>*c*<sub>*i*</sub></sub> is the magnetic field due to coil *c*<sub>*i*</sub>, and the integration is carried over all space. From this,  
 98 typically large set of coil-current patterns, we obtain a practical set by forming an *n*-by-*m* matrix *C* in which  
 99 the coil-current patterns are columns,

$$\mathbf{C} = [\mathbf{c}_1 \mathbf{c}_2 \dots \mathbf{c}_m] ,$$

100 computing its singular-value decomposition,

$$\mathbf{C} = \mathbf{U} \mathbf{\Sigma} \mathbf{V}^T,$$

101 and then taking the first  $N$  left singular vectors  $\mathbf{u}_i$ . Each of these singular vectors describes a coil-current  
 102 pattern. When  $N$  is sufficiently large, linear combinations of  $\mathbf{u}_i$  ( $i = 1 \dots N$ ) can approximate any of the  
 103 original coil-current patterns  $\mathbf{c}_i$  ( $i = 1 \dots m$ ).

104 Each singular vector  $\mathbf{u}_i$  ( $i = 1 \dots N$ ) corresponds to a stream function that describes a particular transducer  
 105 coil. As the  $\mathbf{u}_i$  are mutually orthogonal, we can expect the corresponding coils to have near-zero mutual  
 106 inductances. The coil windings can be extracted from the stream functions as in Refs. [18, 19]: the  
 107 individual turns of the windings follow the isolines of the stream functions, and the windings are obtained  
 108 by connecting consecutive turns in a spiral-like fashion. However, as all coils are described in a common  
 109 basis, their windings typically intersect; we can obtain feasible coil windings by adding a unique offset to  
 110 each coil surface before extracting the windings. When offsetting a surface, it is useful to re-compute the  
 111 respective stream function to ensure that the E-field remains intact. This can be done by computing on the  
 112 shifted surface the minimum-energy coil that induces the same E-field distribution as the original  
 113 (unshifted) stream function using the single-coil optimisation method [19]. If there are a few thin coils, the  
 114 re-optimisation makes typically little difference, and one can simply translate the stream functions (or the  
 115 coil windings) by the required few millimetres. Note that the order of the coils affects the total efficiency of  
 116 a transducer. As a rule of thumb, coils with the smallest characteristic size are most sensitive to the offset  
 117 and should be placed closest to the head if all coils require similar maximum power levels—otherwise, coils  
 118 with the lowest maximum power level can be placed farthest from the head. The number of turns in each  
 119 coil can be selected independently. However, the maximum number of turns in one layer is limited by the  
 120 wire thickness; if the desired level of inductance cannot be reached with this number of turns, inductance  
 121 may be increased by adding turns of wire in series in another layer.

122 Thus, our algorithm to find a set of coil windings is as follows:

- 123 1. Form an evenly discretised set of stimulation patterns from the set of all desired stimulation  
 124 patterns and build optimisation constraints for each pattern.

- 125 2. Select a suitable overall transducer shape. With a common basis, compute the stream function for  
126 the minimum-energy current pattern for each desired stimulation pattern.
- 127 3. Concatenate the stream functions that describe the minimum-energy coils into a matrix (the  
128 stream functions as its columns) and compute its singular value decomposition. Select the first  $N$   
129 (here,  $N = 2$ ) left singular vectors.
- 130 4. Test if the desired set of stimulation patterns can be sufficiently reproduced with the selected  
131 vectors. If not, either increase  $N$  or reduce the extent of the desired set of stimulation patterns.
- 132 5. Build  $N$  overlapping coil surfaces separated by the height of the coil windings. For each surface,  
133 design a minimum-energy coil producing the same E-field distribution as one of the coils described  
134 by the singular vectors.

135 We investigated the performance of the algorithm by designing transducers that can translate the  
136 stimulated spot within various regions. First, we determined a set of coils that can control both the  
137 orientation and location of the stimulated spot within a small region of the brain (similar to the region  
138 accessible with a lattice of 16 small round coils). We computed the induced E-field in the cortex in a  
139 spherical head model with 70-mm cortical radius and 85-mm outer radius using an analytical closed-form  
140 solution [20] and reciprocity [21], and used a large planar surface for the overall transducer shape. The  
141 computed stream functions matched the E-field distribution of a Magstim 70mm Double Coil (The Magstim  
142 Co Ltd, [www.magstim.com](http://www.magstim.com)) that was modelled based on the model by Thielscher and Kammer [22]. The  
143 coil was translated and rotated to stimulate different spots within a rectangular region, the size of which  
144 was increased until the required number of coils increased. The points in the region were sampled from a  
145 geodesic polyhedron whose edge lengths ranged from 2.4 to 2.9 mm. In each point, the different  
146 orientations were sampled with 30° steps, and the focality constraints for each E-field distribution were  
147 defined at 70, 90, 95, 99, and 100 % of the peak E-field. Second, we studied how the number of coils  
148 increases when the surface area of the accessible region is doubled. Third, we investigated a limiting case  
149 by designing a transducer for the stimulation of the whole superficial cortex, with a coil surface that covers  
150 the scalp in a spherically symmetric head model (i.e., a hemispherical surface). Note that, although in this



151 study we applied the spherically symmetric head geometry, the design formalism applies also to realistic  
152 head geometry [19]. In this study, we calculated E-fields in a spherical head model as opposed to a realistic  
153 head model, as these two approaches produce nearly identical coils for the stimulation of motor areas (see  
154 [18, 19]). In addition, coil optimisation in the spherical head model requires only about 1 % of the  
155 computation time compared to that with realistic head models. The much faster computation is mainly due  
156 to much simpler 2-dimensional focality constraints (in each discretisation point, 16 and 162 linear  
157 constraints are required to approximate the constraint for the E-field magnitude in 2 and 3 dimensions,  
158 respectively, see Ref. [19]).

### 159 Two-coil transducer design and implementation

160 We designed and built a multi-locus transducer that can translate the stimulated spot along a 30-mm-long  
161 line segment perpendicular to the direction of the peak E-field. When designing this mTMS transducer, we  
162 computed the induced E-field in the geometry described in the previous section, used a large planar surface  
163 for the overall transducer shape, and computed 31 stream functions to match the E-field distribution of a  
164 Magstim 70mm Double Coil that was translated to stimulate different spots from -15 to 15 mm in 1-mm  
165 steps. The focality constraints for each E-field distribution were defined at 70, 90, 95, 99, and 100 % of the  
166 peak E-field. The first two singular vectors ( $\mathbf{u}_1$  and  $\mathbf{u}_2$ ) explained most (88 %) of the variance in this 31-  
167 dimensional system. We extracted coil windings from these two vectors, with the number of turns selected  
168 so that the inductance of both coils with two strands of wire per turn in series was between 16 and 18  $\mu\text{H}$ .  
169 The oval coil, described by  $\mathbf{u}_2$ , was translated outwards by 4 mm to avoid intersecting windings.

170 We manufactured a coil former from a 10-mm-thick 300-by-200-mm-wide sheet of polyvinyl chloride  
171 following the description of Ref. [19]. The wiring of the figure-of-eight coil was placed at the bottom of  
172 machined 9-mm-deep grooves; the oval coil was wound on top of it in 5-mm-deep grooves. Each coil had  
173 two strands of Litz wire (70 circular 0.2-mm-thick strands, Rudolf Pack GmbH & Co. KG, www.pack-  
174 feindraehte.de) in series. Finally, the wires were glued with epoxy and connected to coil cables. The

175 transducer was finished by assembling a 5-mm-thick polyvinyl-chloride lid with an attached commercial  
176 navigation unit (Nexstim eXimia Navigated Brain Stimulation System, [www.nexstim.com](http://www.nexstim.com)).

### 177 mTMS device

178 We also designed and built a two-channel mTMS device. The device comprises control and power  
179 electronics for both channels, which are essentially copies of our custom-made TMS design [19]. This mTMS  
180 device allows similar pulse waveforms in both coils: it features controllable-pulse-waveform electronics  
181 similar to the design of Peterchev et al. [23] with high capacitance and near-rectangular pulse waveforms,  
182 the pulse duration being independent of the coil inductance. The device comprises two insulated-gate  
183 bipolar transistor (ABB 5SNA 1500E330305, [www.abb.com](http://www.abb.com)) H-bridge circuits with one 1020- $\mu$ F capacitor  
184 (Electronicon E50.R34-105NT0, [www.electronicon.com](http://www.electronicon.com)) for each. In addition to the H bridges, the system  
185 has a common high-voltage power supply (Lumina Power CCPF-2000, [www.luminapower.com](http://www.luminapower.com)), which is  
186 shared between the two channels via a custom-made solid-state relay board, and a common control with a  
187 real-time field-programmable gate array hardware (National Instruments PXI-7841R, [www.ni.com](http://www.ni.com)). Both  
188 capacitors have their own resistive discharge systems. The mTMS device is interfaced with a custom-made  
189 LabVIEW program (National Instruments).

### 190 Validation

191 We used our TMS-coil characteriser [24], which provides E-field values in a spherical head model with 70-  
192 mm cortical radius and 85-mm outer radius, to measure E-field distributions of the two-coil transducer  
193 when driven by our mTMS device. These measurements were used to determine the mutual inductance  
194 between the two coils and to fine-tune the coil voltages to obtain the same E-field intensity for all  
195 translations. In addition, we measured the E-field distributions of each coil individually (with the other coil  
196 disconnected from the device) to estimate the accuracy of the manufacturing process of the coils.

### 197 *In-vivo* demonstration

198 Two healthy males (33 and 28 years old, one left-handed) with no contraindication for TMS participated in  
199 the study after giving their written informed consents. The study was approved by the Coordinating Ethics

200 Committee of the Hospital District of Helsinki and Uusimaa and was carried out in accordance with the  
201 Declaration of Helsinki.

202 During the study, the subject sat in a chair and was instructed to keep his right hand relaxed. We recorded  
203 electromyography (EMG) from the right *abductor pollicis brevis* (APB) muscle with surface electrodes  
204 connected to an EMG device (Nexstim eXimia). The device had a 500-Hz low-pass filter and 3,000-Hz  
205 sampling frequency.

206 First, using only the figure-of-eight coil and physically moving the two-coil transducer, we determined the  
207 right APB hotspot by finding the location in the left primary motor cortex that produced the largest motor-  
208 evoked potentials (MEP) at a given stimulation intensity. Then, we measured the resting motor threshold  
209 (RMT) as the lowest stimulation intensity that produced MEPs greater than or equal to 50  $\mu$ V in peak-to-  
210 peak amplitude in at least 10 out of 20 consecutive trials [25]. Finally, we mapped the APB motor  
211 representation area in two ways: (1) Conventional mapping was carried out by using only the figure-of-  
212 eight coil and physically moving the two-coil transducer to stimulate different targets around the APB  
213 hotspot (a total of 150 pulses). (2) Electronically controlled mapping was conducted by holding the coil in  
214 place and electronically translating the stimulated spot in randomised order from  $-15$  to  $15$  mm relative to  
215 the APB hotspot in 1-mm steps (a total of 124 pulses). In both mappings, the stimulation intensity  
216 was 110 % RMT. For subject 1, the conventional mapping was performed first, whereas for subject 2, the  
217 electronic mapping was performed first. All TMS pulses delivered with our custom-made mTMS device  
218 were monophasic with a 60- $\mu$ s rise time and a 30- $\mu$ s “hold period” of near-constant current [26]; the  
219 interstimulus interval was randomised between 4 and 6 s.

220 The transducer position relative to the head was measured with a neuronavigation system (Nexstim eXimia  
221 Navigated Brain Stimulation System). This system was used both to estimate the stimulated spots in the  
222 conventional mapping and to maintain a constant coil position and orientation during the RMT  
223 measurement and during the electronic mapping. The apparent change in the location of the stimulated  
224 spot was defined as the Cartesian distance between the predicted cortical locations of the E-field maximum

225 in the cortex. In the navigation software, we selected the most similar coil to our figure-of-eight coil, the  
226 Magstim 70mm Double Coil.

227 We rejected trials containing muscle preactivation, artefacts, or noise exceeding  $\pm 10 \mu\text{V}$  in amplitude in the  
228 100-ms time window preceding TMS (a total of 2 out of 548 trials were rejected); in addition, we rejected  
229 the trials in which the coil location was not recorded (a total of 4 out of the remaining 546 trials were  
230 rejected). In the accepted trials, we determined the MEP peak-to-peak amplitudes. To assess the similarity  
231 of the conventional and electronic mapping, for both subjects, we determined the width of a region that  
232 produced MEPs greater than or equal to  $50 \mu\text{V}$  in peak-to-peak amplitude. First, we took the moving  
233 median of ten consecutive responses. Then, to account for possibly discontinuous regions, we computed  
234 the distances between the farthest-from-origin points with median greater than or equal to  $50 \mu\text{V}$  and the  
235 closest-to-origin points with median less than  $50 \mu\text{V}$ . Finally, we defined the width of the region as the  
236 mean of these two distances. We compared the widths obtained by conventional and electronic mapping  
237 with a permutation test (1000 repetitions, uncorrected two-tailed comparison). The level of statistical  
238 significance was chosen to be  $P < 0.05$ .

## 239 Results

### 240 Transducer design algorithm

241 For controlling both the stimulation direction and the location of the stimulated spot within a relatively  
242 small region of the cortex, the algorithm yields a set of five overlapping coils: two figure-of-eight coils at a  
243  $90^\circ$  angle, a circular coil, and two four-leaf-clover coils at a  $45^\circ$  angle (Fig. 1). The possible E-field maxima  
244 produced by this set of coils cover a cortical region of approximately 30-by-30  $\text{mm}^2$ .

245 All five coils of the transducer shown in Fig. 1 resemble coils that have been used for TMS [1, 7] or magnetic  
246 nerve stimulation [27] and are also reasonably efficient unlike small circular coils. From this five-coil set,  
247 three useful two-coil subsets can be identified. (1) Two figure-of-eight coils can control the orientation of  
248 the stimulation (Fig. 1a,b). (2) A figure-of-eight coil and a matched four-leaf-clover coil can control the

249 location of the stimulated spot in the direction parallel to the stimulation direction (e.g., Fig. 1a,e). (3) A  
250 figure-of-eight coil and a matched, somewhat circular coil can control the location of the stimulated spot in  
251 the direction perpendicular to the stimulation direction (e.g., the coil in Fig. 1a and a coil formed by  
252 merging the coils in Fig. 1c,d; see Fig. 2). As the primary motor cortex is often stimulated in the direction  
253 perpendicular to the central sulcus, this last pair alone would already provide most of the desired control  
254 over the stimulated spot in the primary motor cortex.

255 In addition to smaller regions of interest, the algorithm is suitable for designing optimised coil sets for  
256 larger regions of interest. For example, the size of the covered region can be doubled by increasing the  
257 number of coils from five to eight. When one applies this algorithm to design a transducer for a wide region  
258 of interest, e.g., the whole superficial cortex, with a coil surface that covers the scalp, the algorithm gives a  
259 set of increasingly complicated TMS coils, each of which would cover the whole transducer surface. With  
260 typical TMS focality constraints, about 50–70 such coils would suffice for adequate control. In this case, an  
261 orthogonal varimax rotation [28] of the coil-current patterns may be used to minimise their overlap and  
262 yield an array of small (near-) circular coils more suitable for practical implementation. Neighbours of such  
263 algorithmically designed small coils overlap by about 10 % to remain orthogonal and to provide smooth  
264 control over the stimulated spot. In addition, the coils at the edge of the array have about twice the surface  
265 area of the other coils.

## 266 Two-coil transducer

267 The two-coil transducer that can translate the stimulated spot along a 30-mm-long line segment  
268 perpendicular to the stimulation direction resembles a figure-of-eight coil overlaid by an oval coil (Fig. 2).  
269 Our figure-of-eight coil alone produces an E-field distribution similar to that of conventional figure-of-eight  
270 coils (Fig. 3b, solid purple line), whereas the oval coil produces a bimodal field distribution along its left–  
271 right axis, with opposite E-field directions (Fig. 3b, dashed green line). A superposition of these two E-fields  
272 can translate the peak induced E-field along the left–right axis of the transducer (e.g., as in Fig. 3b dotted

273 black line). If the coil voltages in both coils are selected appropriately (Fig. 3a), we can maintain constant  
274 peak intensity while moving the stimulated spot steplessly (Fig. 3c).

275 The voltages shown in Fig. 3a were fine-tuned to compensate for the non-zero mutual inductance between  
276 the two coils, which we estimated to be around 0.02 times the coil inductance. The manufacturing process  
277 produced coils that were highly similar with their corresponding simulated properties: both measured field  
278 distributions in the direction perpendicular to the peak induced E-field of the figure-of-eight coil (Fig. 3b)  
279 are almost indistinguishable from the corresponding simulated spatial distributions of the coil windings  
280 (correlation 0.998 for the figure-of-eight coil and 0.999 for the oval coil).

### 281 *In-vivo* demonstration

282 The conventional and the electronically controlled maps of the APB motor representation area had similar  
283 extent for both subjects, as seen in Fig. 4. For subject 1, the widths of the regions producing MEPs greater  
284 than or equal to 50  $\mu$ V in peak-to-peak amplitude at 110 % RMT in the conventional and electronic  
285 mappings were 13.7 and 16.8 mm, respectively. The difference between these two values was not  
286 statistically significant (uncorrected two-tailed  $P = 0.074$ ). For subject 2, the respective values were 15.7  
287 and 15.3 mm (uncorrected two-tailed  $P = 0.83$ ). For subject 2, the maps are also visually essentially  
288 indistinguishable; for subject 1, the electronic map appears slightly wider than the conventional map.  
289 Ideally, the conventional and electronic mapping results should be similar to each other.

## 290 Discussion

291 We have proposed and demonstrated a practical approach to mTMS: overlapping coils forming a single  
292 transducer enable stepless electronic selection of the stimulated spot. This approach differs considerably  
293 from the previously suggested approach of having an array of adjacent coils [8, 16], which would require  
294 considerably more channels in particular for the minimum viable array size. In addition, to allow stepless  
295 control over the stimulated spot, those adjacent coils would have to be relatively small and therefore  
296 inefficient—each of them alone would require similar levels of power as a single conventional TMS coil. The

297 proposed approach solves both limitations; thus, with just two overlapping coils, we could build the  
298 simplest instance of an electronically controlled mTMS device that allows shifting the stimulated spot while  
299 keeping the E-field profile essentially unchanged.

300 Our *in-vivo* demonstration of the electronic stimulation targeting showed that physical transducer  
301 movement can be substituted with electronic targeting. For subject 2, the two mapping approaches  
302 produced practically identical results. The slight differences in the mapping results of subject 1 may be due  
303 to several reasons, e.g., a higher excitability of the M1 during the electronic mapping. Indeed, the  
304 electronic mapping produced larger responses than the conventional mapping at the cortical location 0  
305 (see Fig. 4a) although this corresponds to identical stimulation with the figure-of-eight coil only in both  
306 methods.

307 The electronic control can be made near instantaneous compared to the time scales at which the brain  
308 functions; the described mTMS device can stimulate separate cortical targets with interstimulus intervals  
309 down to around 0.3 ms (the lower limit of the interstimulus interval is given by the TMS-pulse duration).  
310 Thus, electronically controlled mTMS allows, for example, studying short-distance interactions between  
311 inhibitory and facilitatory circuits [14] in detail. When combined with physiological or behavioural  
312 recordings, mTMS would allow implementing also closed-loop paradigms [29, 30, 31], in which the  
313 stimulation targets and timings of subsequent pulses would be derived, e.g., from real-time-analysed  
314 electroencephalography data.

315 In addition to its impact on neuroscience, the ability to select different stimulation targets without any  
316 physical movement of the transducer may revolutionise also clinical TMS. mTMS will allow, e.g., electronic  
317 stabilisation to compensate for minor patient movements during a treatment session. This would reduce  
318 the stress of manual effort required to maintain the correct coil position. In addition, mTMS devices with  
319 electronic control over the stimulated spot would allow automating clinical procedures in which cortical  
320 areas are mapped, e.g., before brain surgery [32, 33]. With the development of new mTMS paradigms, we  
321 anticipate that mTMS will lead to new clinical applications.

## 322 Conclusions

323 We developed an algorithm to design practical mTMS transducers capable of electronic stimulation  
324 targeting and demonstrated such a transducer *in vivo*.

## 325 Acknowledgements

326 This work was supported by the Finnish Cultural Foundation and the Academy of Finland (Decision Nos.  
327 255347, 265680, and 294625). The coil former parts were manufactured by Enna Rane (Aalto University  
328 Design Factory). The coil cables and their connectors were donated by Nexstim Plc. We acknowledge the  
329 computational resources provided by the Aalto Science-IT project.

## 330 Conflict-of-interest statement

331 The authors are inventors on patent applications on mTMS technology. J.O.N. has received unrelated  
332 consulting fees from Nexstim Plc., and R.J.I. is an advisor and a minority shareholder of the company.

## 333 References

- 334 [1] Barker AT, Jalinous R, Freeston IL. Non-invasive magnetic stimulation of human motor cortex. *Lancet*  
335 1985;325:1106–7.
- 336 [2] Massimini M, Ferrarelli F, Huber R, Esser SK, Singh H, Tononi G. Breakdown of cortical effective  
337 connectivity during sleep. *Science* 2005;309:2228–32.
- 338 [3] Reis J, Swayne OB, Vandermeeren Y, Camus M, Dimyan MA, Harris-Love M, et al. Contribution of  
339 transcranial magnetic stimulation to the understanding of cortical mechanisms involved in motor control. *J*  
340 *Physiol* 2008;586:325–51.
- 341 [4] Rose NS, LaRocque JJ, Riggall AC, Gosseries O, Starrett MJ, Meyering EE, et al. Reactivation of latent  
342 working memories with transcranial magnetic stimulation. *Science* 2016;354:1136–39.



- 343 [5] Berlim MT, van den Eynde F, Tovar-Perdomo S, Daskalakis ZJ. Response, remission and drop-out rates  
344 following high-frequency repetitive transcranial magnetic stimulation (rTMS) for treating major depression:  
345 a systematic review and meta-analysis of randomized, double-blind and sham-controlled trials. *Psychol*  
346 *Med* 2014;44:225–39.
- 347 [6] Lefaucheur JP, Picht T. The value of preoperative functional cortical mapping using navigated TMS. *Clin*  
348 *Neurophysiol* 2016;46:125–33.
- 349 [7] Ueno S, Tashiro T, Harada K. Localized stimulation of neural tissues in the brain by means of a paired  
350 configuration of time-varying magnetic fields. *J Appl Phys* 1988;64:5862–64.
- 351 [8] Ruohonen J, Ilmoniemi RJ. Multichannel magnetic stimulation: improved stimulus targeting. *Adv Occup*  
352 *Med Rehabil* 1996;2:55–64.
- 353 [9] Ettinger GJ, Leventon ME, Grimson WEL, Kikinis R, Gugino L, Cote W, et al. Experimentation with a  
354 transcranial magnetic stimulation system for functional brain mapping. *Med Image Anal* 1998;2:133–42.
- 355 [10] Karhu J, Hannula H, Laine J, Ruohonen J. Navigated transcranial magnetic stimulation: principles and  
356 protocol for mapping the motor cortex. In: Rotenberg A, Horvath JC, Pascual-Leone A, editors. *Transcranial*  
357 *Magnetic Stimulation*, New York: Springer; 2014, p. 337–59.
- 358 [11] Kantelhardt SR, Fadini T, Finke M, Kallenberg K, Siemerikus J, Bockermann V, et al. Robot-assisted  
359 image-guided transcranial magnetic stimulation for somatotopic mapping of the motor cortex: a clinical  
360 pilot study. *Acta Neurochir* 2010;152:333–43.
- 361 [12] Kujirai T, Caramia MD, Rothwell JC, Day BL, Thompson PD, Ferbert A, et al. Corticocortical inhibition in  
362 human motor cortex. *J Physiol* 1993;471:501–19.
- 363 [13] Arai N, Müller-Dahlhaus F, Murakami T, Bliem B, Lu MK, Ugawa Y, et al. State-dependent and timing-  
364 dependent bidirectional associative plasticity in the human SMA-M1 network. *J Neurosci* 2011;31:15376–  
365 83.

- 366 [14] Ziemann U, Rothwell JC, Ridding MC. Interaction between intracortical inhibition and facilitation in  
367 human motor cortex. *J Physiol* 1996;496:873–81.
- 368 [15] Bäumer T, Schippling S, Kroeger J, Zittel S, Koch G, Thomalla G, et al. Inhibitory and facilitatory  
369 connectivity from ventral premotor to primary motor cortex in healthy humans at rest—a bifocal TMS study.  
370 *Clin Neurophysiol* 2009;120:1724–31.
- 371 [16] Ilmoniemi RJ, Grandori F. Device for applying a programmable excitation electric field to a target.  
372 Patent FI 100458 B, filed 13th October 1993, issued 15th December 1997.
- 373 [17] Roth BJ, Maccabee PJ, Eberle LP, Amassian VE, Hallett M, Cadwell J, et al. In vitro evaluation of a 4-leaf  
374 coil design for magnetic stimulation of peripheral nerve. *Electroencephalogr Clin Neurophysiol* 1994;93:68–  
375 74.
- 376 [18] Koponen LM, Nieminen JO, Ilmoniemi RJ. Minimum-energy coils for transcranial magnetic stimulation:  
377 application to focal stimulation. *Brain Stimul* 2015;8:124–34.
- 378 [19] Koponen LM, Nieminen JO, Mutanen TP, Stenroos M, Ilmoniemi RJ. Coil optimisation for transcranial  
379 magnetic stimulation in realistic head geometry. *Brain Stimul* 2017;10:795–805.
- 380 [20] Sarvas J. Basic mathematical and electromagnetic concepts of the biomagnetic inverse problem. *Phys*  
381 *Med Biol* 1987;32:11–22.
- 382 [21] Heller L, van Hulsteyn DB. Brain stimulation using electromagnetic sources: theoretical aspects.  
383 *Biophys J* 1992;63:129–38.
- 384 [22] Thielscher A, Kammer T. Linking physics with physiology in TMS: a sphere field model to determine the  
385 cortical stimulation site in TMS. *NeuroImage* 2002;17:1117–30.
- 386 [23] Peterchev AV, D’Ostilio K, Rothwell JC, Murphy DL. Controllable pulse parameter transcranial magnetic  
387 stimulator with enhanced circuit topology and pulse shaping. *J Neural Eng* 2014;11:056023.

- 388 [24] Nieminen JO, Koponen LM, Ilmoniemi RJ. Experimental characterization of the electric field distribution  
389 induced by TMS devices. *Brain Stimul* 2015;8:582–89.
- 390 [25] Rothwell JC, Hallett M, Berardelli A, Eisen A, Rossini P, Paulus W. Magnetic stimulation: motor evoked  
391 potentials. *Electroencephalogr Clin Neurophysiol Suppl* 1999;52:97–103.
- 392 [26] Koponen LM, Nieminen JO, Mutanen TP, Ilmoniemi RJ. Non-invasive extraction of microsecond-scale  
393 dynamics from human motor cortex. *Hum Brain Mapp*. In press.
- 394 [27] Roth Y, Levkovitz Y, Pell GS, Ankry M, Zangen A. Safety and characterization of a novel multi-channel  
395 TMS stimulator. *Brain Stimul* 2014;7:194–205.
- 396 [28] Kaiser HF. The varimax criterion for analytic rotation in factor analysis. *Psychometrika* 1958;23:187–  
397 200.
- 398 [29] Bergmann TO, Karabanov A, Hartwigsen G, Thielscher A, Siebner HR. Combining non-invasive  
399 transcranial brain stimulation with neuroimaging and electrophysiology: current approaches and future  
400 perspectives. *NeuroImage* 2016;140:4–19.
- 401 [30] Zrenner C, Belardinelli P, Müller-Dahlhaus F, Ziemann U. Closed-loop neuroscience and non-invasive  
402 brain stimulation: a tale of two loops. *Front Cell Neurosci* 2016;10:92.
- 403 [31] Zrenner C, Desideri D, Belardinelli P, Ziemann U. Real-time EEG-defined excitability states determine  
404 efficacy of TMS-induced plasticity in human motor cortex. *Brain Stimul* 2018;11:374–89.
- 405 [32] Picht T, Schmidt S, Brandt S, Frey D, Hannula H, Neuvonen T, et al. Preoperative functional mapping for  
406 rolandic brain tumor surgery: comparison of navigated transcranial magnetic stimulation to direct cortical  
407 stimulation. *Neurosurgery* 2011;69:581–9.
- 408 [33] Picht T, Krieg SM, Sollmann N, Rösler J, Niraula B, Neuvonen T, et al. A comparison of language  
409 mapping by preoperative navigated transcranial magnetic stimulation and direct cortical stimulation during  
410 awake surgery. *Neurosurgery* 2013;72:808–19.

## 411 Figures

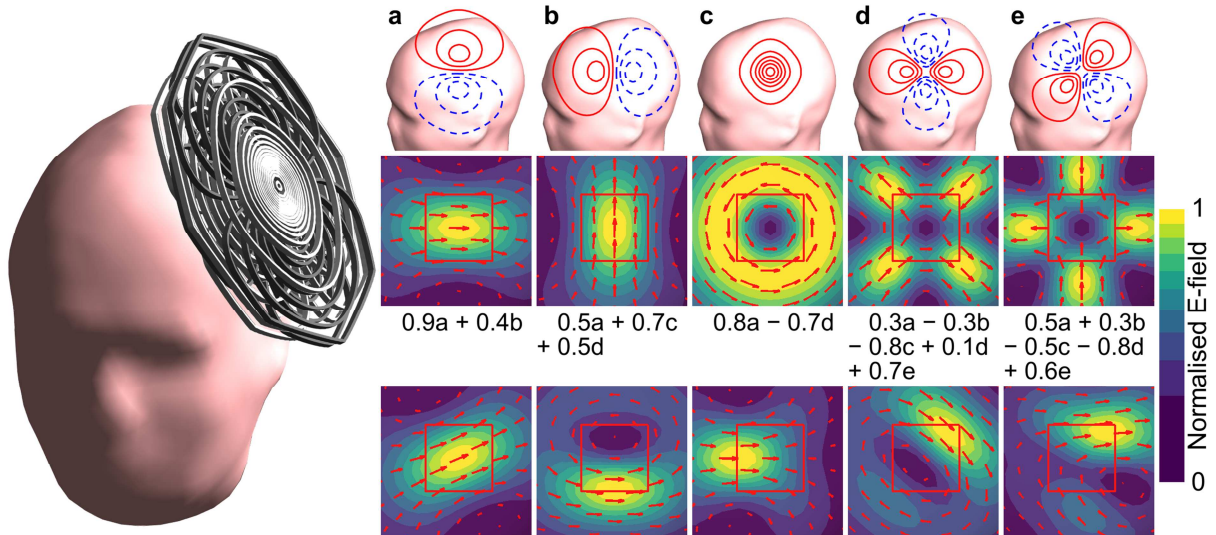
412 **Figure 1. Five-coil mTMS transducer.** With five coils, the location of the stimulated spot can be moved in  
413 both tangential directions and the stimulation direction can be freely selected. **(a–e)** The coil windings of  
414 each coil are shown with a reduced number of turns for increased clarity. The solid red and the dashed blue  
415 windings carry current in clockwise and counter-clockwise directions for positive coil voltages, respectively.  
416 Each coil induces a distinct E-field distribution in the cortex (middle row). Their superpositions produce the  
417 desired stimuli, some examples of which are shown in the bottom row. The side lengths of the red squares  
418 are 30 mm. The E-field distributions were computed in the spherical head model described in section  
419 “Transducer design algorithm” and a realistic head model is used to illustrate better the size of the resulting  
420 coils. The visualisation on the left shows all five coils assembled into a single transducer; in the visualisation,  
421 the coils are in order e–d–b–a–c to maximise the total system efficiency.

422 **Figure 2. Two-coil mTMS transducer.** Our transducer consists of a minimum-energy figure-of-eight coil and  
423 an overlapping oval coil. The figure-of-eight coil alone produces a focal stimulus underneath the centre of  
424 the transducer. The oval coil alone produces a relatively broad stimulus on both sides of that location, with  
425 the E-field reversing its direction underneath the centre of the transducer. As a superposition of the fields  
426 of the two coils, we obtain a focal stimulus to the desired target near the centre. After the photograph was  
427 taken, the wires were glued in place with epoxy.

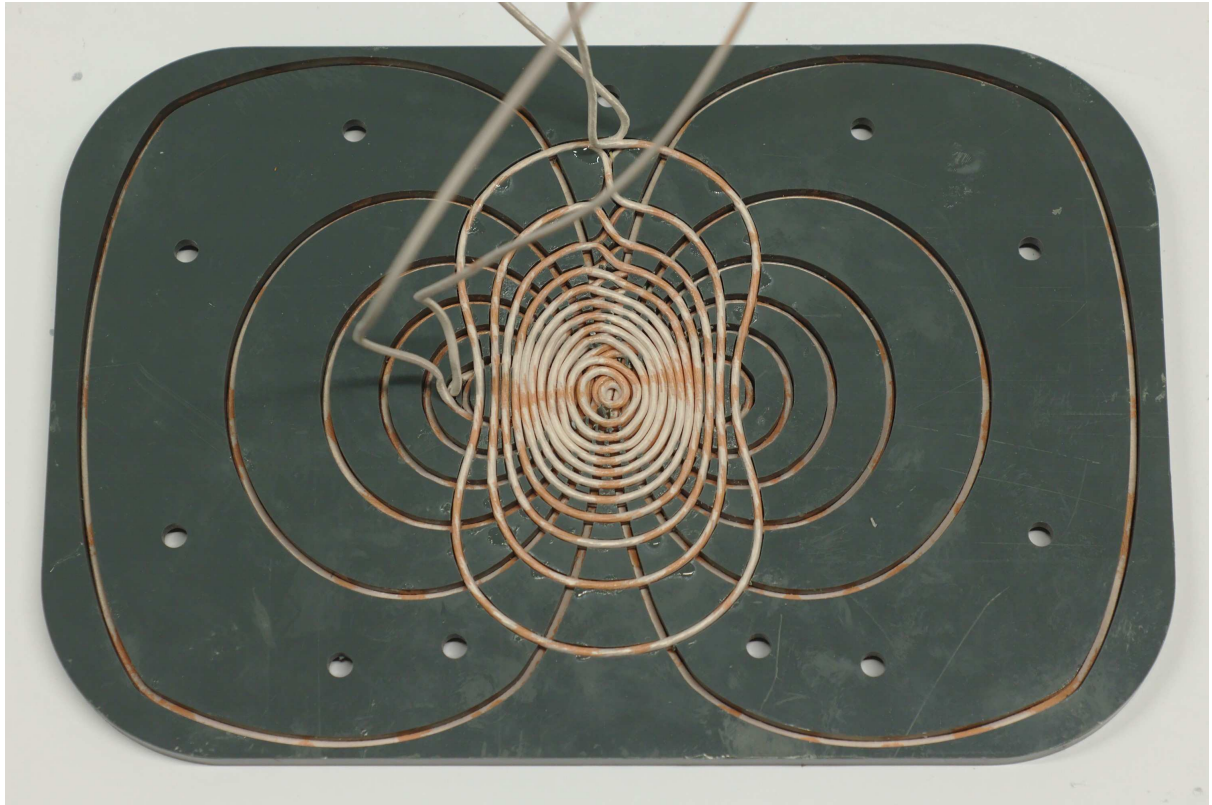
428 **Figure 3. Coil voltage and induced electric field.** The stimulated spot can be adjusted by changing the  
429 voltages that drive the currents to the coils of our mTMS transducer. **(a)** The relationship between the  
430 location of the stimulated spot relative to the transducer centre and the coil voltage in the figure-of-eight  
431 coil is near-parabolic (solid purple curve); for the oval coil, this relationship is near-linear (dashed green  
432 curve). **(b)** A linear superposition of the E-field distributions of the figure-of-eight coil (solid purple line) and  
433 oval coil (dashed green line) produces an E-field distribution whose peak is translated (dotted black line).  
434 Here, the location is measured along a curved line perpendicular to the peak induced E-field in a spherical  
435 phantom. In **(a)** and **(b)**, the vertical dashed lines indicate the location of the stimulated spot of panel **(b)**.

436 **(c)** The measured E-field distribution along a curved line perpendicular to the peak induced E-field in a  
437 spherical phantom when the stimulated spot is located at  $-15$ ,  $-10$ ,  $-5$ ,  $0$ ,  $5$ ,  $10$ , and  $15$  mm. When  
438 connected to the mTMS device, the two coils have a non-zero mutual inductance (coupling coefficient of  
439 the order of  $0.02$ ), which has been compensated for in the coil voltages **(a)** to produce constant stimulation  
440 intensity at all target positions **(c)**.

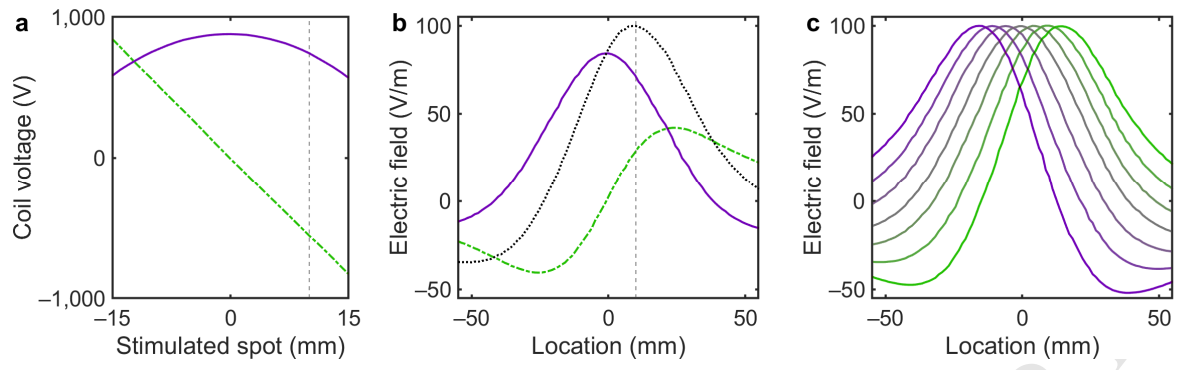
441 **Figure 4. Motor mapping.** Panels **(a)** and **(b)** depict the MEP peak-to-peak amplitudes of subjects 1 and 2 as  
442 a function of the cortical location of the peak induced E-field, respectively. The solid purple lines and the  
443 dashed green lines visualise the conventional and electronic motor representation maps of the APB muscle  
444 (at  $110\%$  RMT), respectively. Each line depicts the median of ten consecutive individual responses,  
445 covering on average  $2$  mm of the cortex. The individual responses of the conventional and electronic  
446 mappings are represented with purple plusses and green crosses, respectively. A motor representation  
447 area (indicated by the horizontal purple and green lines near the top of the panels) is defined as the area in  
448 which the respective median curve is above  $50\ \mu\text{V}$ . The widths of the motor representation areas of the  
449 conventional and electronic maps do not differ in a statistically significant sense ( $P = 0.074$  and  $P = 0.83$   
450 for subject 1 and 2, respectively).



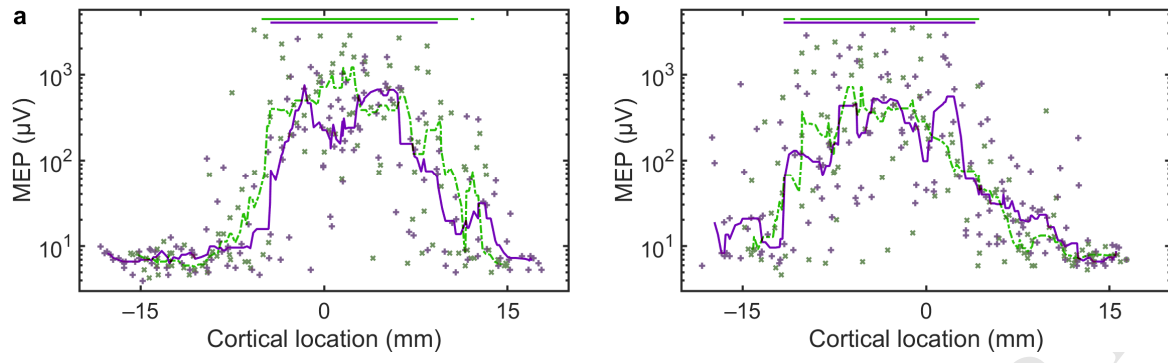
ACCEPTED MANUSCRIPT



ACCEPTED MANUSCRIPT







## Highlights

- Transcranial magnetic stimulation with rapid, electronic stimulation targeting.
- A practical method to change the locus of stimulation without coil movement.
- Demonstration of stimulation of the primary motor cortex with a two-coil device.

ACCEPTED MANUSCRIPT